Chapter 19
Frequency Band Damping: Implementation and Innovations

Dagny Beale, Gregory Bunting, Nathan Crane, David Day, Clark Dohrmann, Payton Lindsay, Justin Pepe, and Julia Plews

Abstract This talk overviews a novel frequency-band-limited approach to tunable structural damping, building on previous work in this area [1]. In particular, this work will discuss numerical stability, practical code implementation considerations, and application to large-scale problems in structural dynamics.

The inclusion of damping in FEA is not merely a theoretical enhancement but a practical necessity. It bridges the gap between idealized representations and realistic structural response. By providing a more flexible approach to damping, we enable engineers and scientists to make fine-tuned, informed decisions in the design, analysis, and optimization of structures.

Keywords Frequency band damping · Frequency dependent damping · Damping models · Modal damping · Damping

Introduction

Finite Element Analysis (FEA) is a cornerstone in the engineering and scientific communities for predicting structural response. An understated yet crucial part of FEA is damping, which can heuristically capture real-world energy dissipation mechanisms in structures. Choice of damping model is critical, and directly influences the fidelity and robustness of the simulation.

Recently, Huang, Sturt, and Willford [1] proposed a novel approach to apply uniform damping across a spectrum of frequencies. The approach enjoys several benefits, including the ability to apply differential damping across subregions of a model.

This work builds upon the original publication's foundation, and details its incorporation into a massively parallel finite element code [2]. It delves more deeply into the derivation and implementation, examines some potential drawbacks of the approach, and proposes a potential path forward towards improving it. We also include an example on a multi-million element model, where we compare the new approach to direct modal damping approaches, explore the performance characteristics of the model, and make some recommendations for usage best practices.

Theory

In this section, we provide a brief overview of the theory of the damping approach, as well as some additional clarifying details and insights beyond what was given in the original paper.

We begin the discussion with the equation of motion, which is given by

$$M\ddot{u}(t) + f_{int}(t) = f_{ext}(t) \tag{1}$$

where the $f_{int}(t)$, the *internal resisting force*, consists of a constitutive and damping component,

$$f_0(t) + f_d(t).$$

Here we assume linear elastic behavior such that $f_0(t) = Ku(t)$, and adopt the notation $d = u(t), v = \dot{u}(t), a = \ddot{u}(t)$.

Dagny Beale · Gregory Bunting · Nathan Crane · David Day · Clark Dohrmann · Payton Lindsay · Justin Pepe · Julia Plews
Sandia National Laboratories, Albuquerque, NM 87185
e-mail: dmbeale@sandia.gov; gbuntin@sandia.gov; nkcrane@sandia.gov; dmday@sandia.gov; crdohrm@sandia.gov; plindsa@sandia.gov; jppepe@sandia.gov; japlews@sandia.gov;

Brandon Dilworth et al. (eds.), *Topics in Modal Analysis & Parameter Identification I, Vol. 9*, Conference Proceedings of the Society for Experimental Mechanics Series, https://doi.org/10.13052/97887-438-0154-2_19

In the frequency domain, the resisting force is defined as

$$F_{int}(\omega) = [K_1(\omega) + iK_2(\omega)]\, U(\omega) \tag{2}$$

We now introduce the concept of a *specific damping factor*, a dimensionless measure of damping given by [1, eqn 3.8.9], [3, eqn (5)]

$$\xi(\omega) = \frac{K_2(\omega)}{K_1(0)} \tag{3}$$

With these prerequisites, we may now restate the main goal of this approach more precisely: define a formulation for the damping force, $f_d(t)$, that approximates a *target specific damping factor* $\xi \approx \eta$ across a frequency range $[\omega_1, \omega_2]$.

Consider a damping force given by the following relation [1, eqn (7)]

$$f_d(t) = \eta \sum_{1}^{N} \frac{2\alpha_n}{\omega_{cn}} \dot{f}_{Ln}(t) \tag{4}$$

where ω_{cn} is the *n*th logarithmically-spaced cutoff frequency between $\omega 1$ and $\omega 2$.

The *n*th filtered force history, $f_{Ln}(t)$, is governed by the relation [1, eqn 9]

$$f_{Ln}(t) + \frac{\dot{f}_{Ln}(t)}{\omega_{cn}} = f_0(t) \tag{5}$$

Calculating the specific damping factor of the damping force given by eq. (4) yields the following result (see appendix A):

$$\xi = \eta \sum_{n=1}^{N} \alpha_n \phi_n(\omega) \tag{6}$$

where $\phi_n(\omega) = \frac{2\omega/\omega_{cn}}{1+(\omega/\omega_{cn})^2}$.

Recalling again the goal of approximating $\xi \approx \eta$ within $[\omega_1, \omega_2]$, we see that an optimal damping force is one which satisfies the following relation:

$$\sum_{n=1}^{N} \alpha_n \phi_n(\omega) \approx 1 \quad \forall \omega \in [\omega_1, \omega_2] \tag{7}$$

Thus, we may formulate the least squares approach to calculate the optimal values of α_n, ultimately leading to the following relations [1, eqns (19),(20)]:

$$\alpha = \mathbb{X}^{-1} \curvearrowright \tag{8}$$

where

$$\begin{aligned} y_i &= \int_{\omega_1}^{\omega_2} \phi_i(\omega) d\omega \\ X_{ij} &= \int_{\omega_1}^{\omega_2} \phi_i(\omega)\phi_j(\omega) d\omega \end{aligned} \tag{9}$$

Although not given in the original paper, the integrals given in eq. (20) can be solved directly, with the following solutions:

$$y_i = \int \phi_i(\omega) d\omega = \omega_{ci} \ln(\omega_{ci}^2 + \omega^2) \tag{10}$$

$$X_{ij} = \int \phi_i(\omega)\phi_j(\omega) d\omega = \begin{cases} 2\omega_c \left(\arctan\left(\frac{\omega}{\omega_c}\right) - \frac{\omega_c \omega}{\omega_c^2+\omega^2}\right) & \text{if } \omega_{ci} = \omega_{cj} = \omega_c \\ \frac{4\omega_{ci}\omega_{cj}}{\omega_{ci}^2-\omega_{cj}^2} \left(\omega_{ci} \arctan\left(\frac{\omega}{\omega_{ci}}\right) - \omega_{cj} \arctan\left(\frac{\omega}{\omega_{cj}}\right)\right) & \text{otherwise} \end{cases} \tag{11}$$

In fig. 1, we explore how well the chosen relation matches the goal ($\sum_{n=1}^{N} \alpha_n \phi_n(\omega) \approx 1$). Figure 1a shows the contributions of each component to the overall sum, and shows good agreement in the frequency range of interest. However, note that the plot is logarithmic in the x-axis, which can obfuscate the slowness of the drop-off outside of the desired range. This slow decay is because the formulation as outlined makes no attempt to minimize damping outside the frequency range of interest, and is one of the key drawbacks of this approach.

Figure 1b demonstrates this aspect more clearly, where there is nearly 20% of the maximum damping an order of magnitude above the high-frequency cutoff. This is an important clarification for potential users of this capability to keep in mind, and can lead to unintended behavior, for example when combining multiple frequency bands.

[1] $\omega_1 = 3.5, \omega_2 = 20, N = 4$

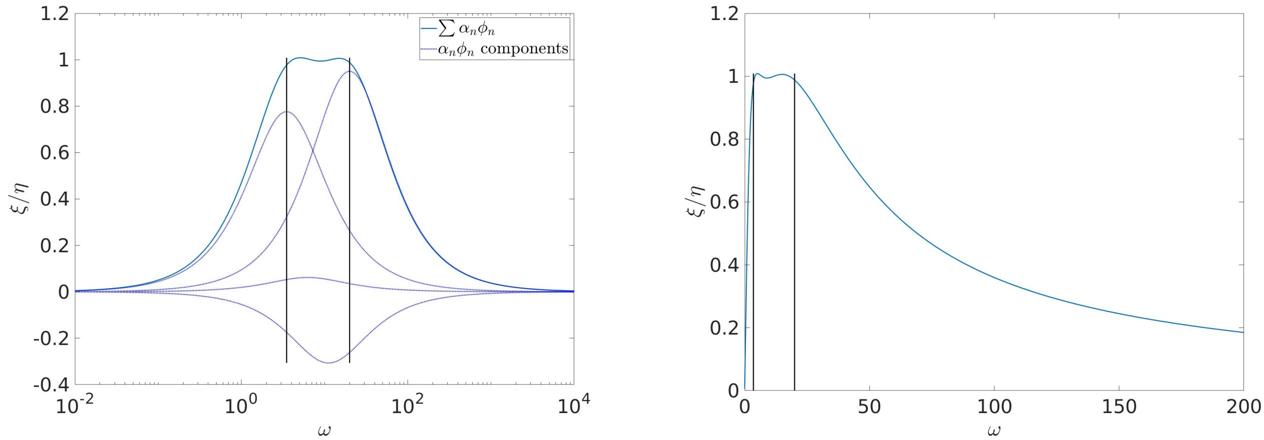

(a) Summation of components.

(b) Linear scale.

Fig. 1 Specific damping factor scale[1].

The results above motivate the need for an improved formulation that not only approximates the target damping within a frequency range, but also minimizes damping outside of it.

One natural modification to accomplish this goal is to optimize α_n to instead satisfy the following relation:

$$\sum_{n=1}^{N} \alpha_n \phi_n(\omega) \approx 1_{[\omega_1,\omega_2]}(\omega) \quad \forall \omega \in [0, \inf] \tag{12}$$

where the *indicator function* $1_{[\omega_1,\omega_2]}(\omega)$ is defined as,

$$1_{[\omega_1,\omega_2]}(\omega) := \begin{cases} 1 & \text{if } \omega \in [\omega_1, \omega_2] \\ 0 & \text{otherwise} \end{cases} \tag{13}$$

This leads to a similar formulation to eq. (8), but with the following definitions for $\mathbb{X}$ and $\curvearrowright$

$$\begin{aligned} y_i &= \int_{\omega_1}^{\omega_2} \phi_i(\omega) d\omega \\ X_{ij} &= \int_{0}^{\inf} \phi_i(\omega)\phi_j(\omega) d\omega \end{aligned} \tag{14}$$

(note the modified range of integration for X_{ij}).

We now regenerate fig. 1 using the above relations. In the resulting plots (fig. 2), while we do see a quick drop-off outside of the target frequency range, the match inside the range is significantly worse, and the scale actually drops below zero at several points, indicating that an intermediate range of integration may be optimal.

To explore this concept, fig. 3 compares the original range of $[\omega_1, \omega_2]$ along with several slightly larger ranges of integration, as well as the full range. These results indicate that separating the choice of integration range from the frequency range of interest is a viable option to address the inherent drawbacks of the existing methodology, and warrants more investigation. This simple modification provides a tunable parameter to choose between the best fit in the frequency range of interest, or the fastest decay outside of it, along with anything in-between.

Relation to viscous damping

In the outlined methodology, the level of damping is controlled by the target specific damping factor η. However, for the sake of usability, it is convenient to express damping in more familiar terms, namely, the viscous damping ratio ζ.

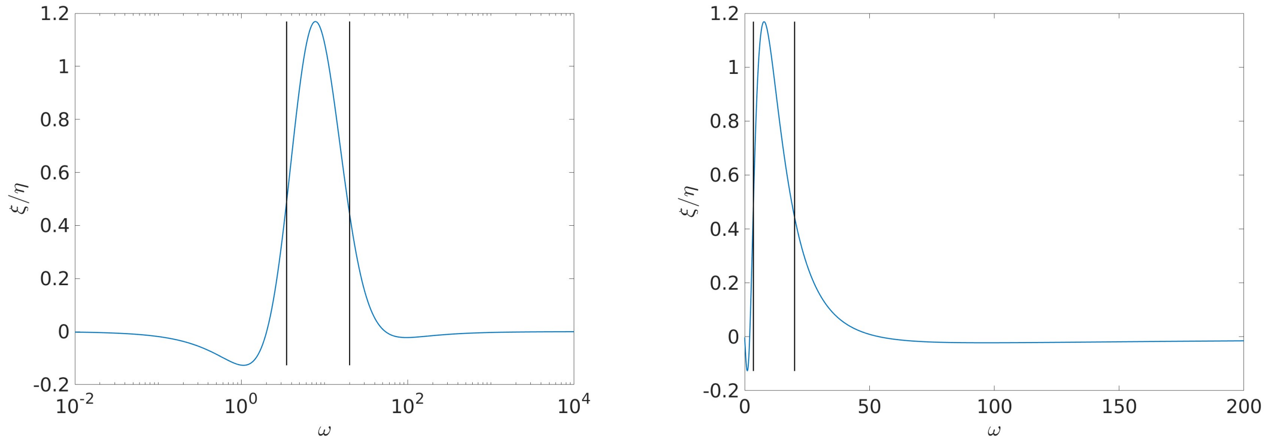

(a) Log scale. (b) Linear scale.

Fig. 2 Specific damping factor scale, modified formulation.

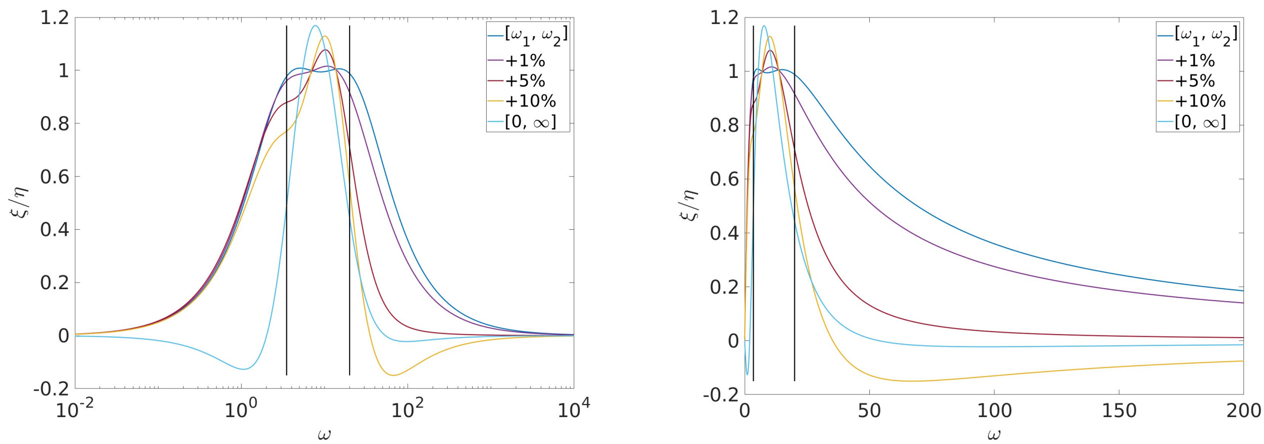

(a) Log scale. (b) Linear scale.

Fig. 3 Specific damping factor scale: range comparison.

The viscous damping ratio ζ may be defined as [1, eqns 5, 6]

$$\zeta = \omega_n \xi/(2\omega)$$
$$\text{or} \tag{15}$$
$$\xi = 2\zeta \frac{\omega}{\omega_n}$$

Plugging eq. (6) into eq. (15), we obtain the following relation:

$$\eta \sum_{n=1}^{N} \alpha_n \phi_n(\omega) = 2\zeta \frac{\omega}{\omega_n} \tag{16}$$

After substituting eq. (7), eq. (16) simplifies to the following, which relates the target specific damping factor η to the viscous damping ratio ζ

$$\eta \approx 2\zeta \frac{\omega}{\omega_n} \tag{17}$$

At the natural frequency ω_n, eq. (17) simplifies even further

$$\eta \approx 2\zeta \tag{18}$$

While eq. (18) is technically only valid at the natural frequency, it provides a comparable level of damping across a wide range of damping ratios, as seen in fig. 4.

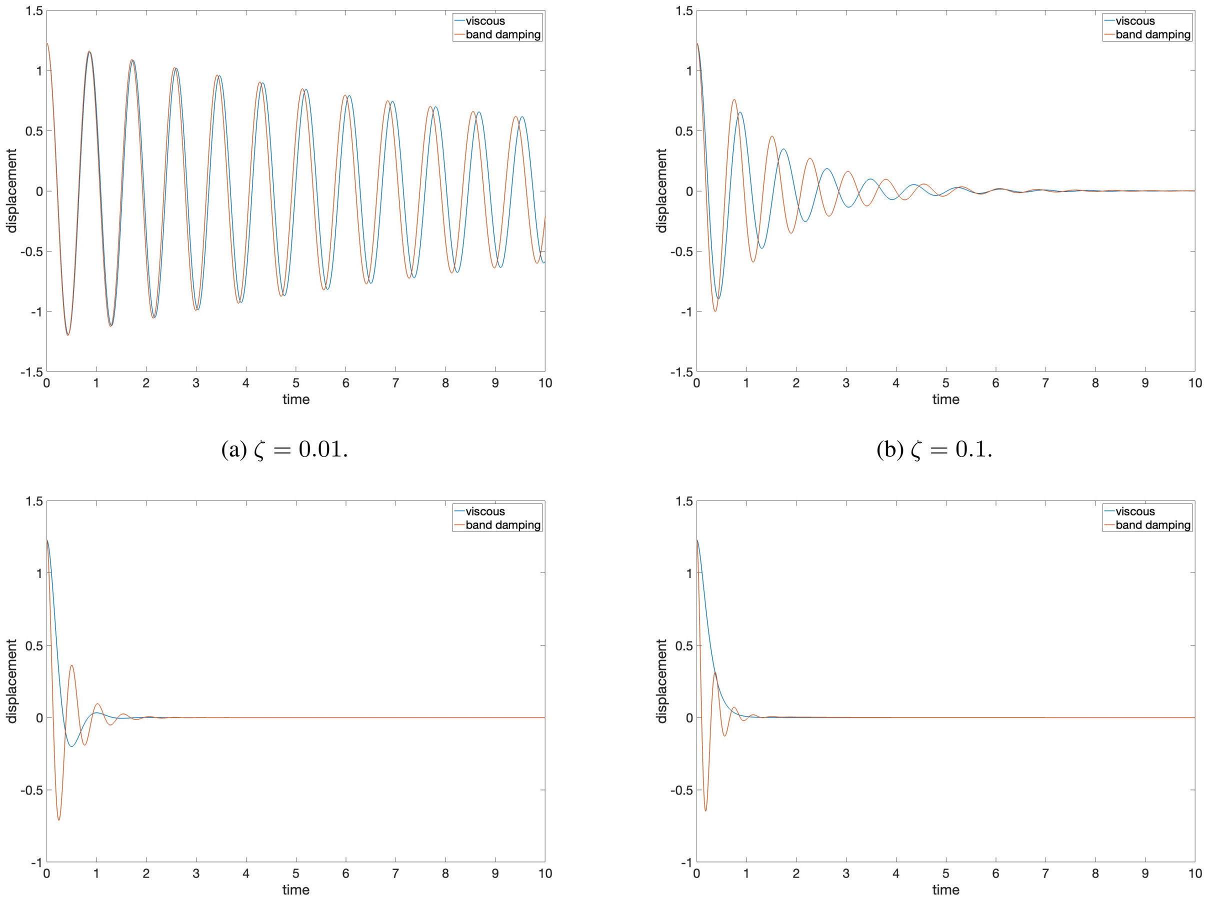

(a) $\zeta = 0.01$.

(b) $\zeta = 0.1$.

(c) $\zeta = 0.5$.

(d) $\zeta = 1$ (critically damped).

Fig. 4 Comparison of band-limited and viscously-damped response[2].

Taking the same system as fig. 4 and fixing $\zeta = 0.1$, we also see that eq. (18) remains a good approximation for a wide range of frequency bands in fig. 5.

Based on these considerations, eq. (18) was chosen to allow the convenient specification of band-limited damping given a desired damping ratio.

As an interesting aside, the band-limited methodology may also be modified to apply viscous damping across a limited frequency range.

To accomplish this, we modify eq. (7) in the following way:

$$\sum_{n=1}^{N} \alpha_n \phi_n(\omega) \approx \frac{\omega}{\omega_n} \quad \forall \omega \in [\omega_1, \omega_2] \tag{19}$$

which again leads to a similar formulation as eq. (8), now with the following definitions for $\mathbb{X}$ and $\curvearrowright$,

$$\begin{aligned} y_i &= \int_{\omega_1}^{\omega_2} \frac{\omega}{\omega_n} \phi_i(\omega) d\omega \\ X_{ij} &= \int_{\omega_1}^{\omega_2} \phi_i(\omega)\phi_j(\omega) d\omega \end{aligned} \tag{20}$$

[2]Spring-mass system in free vibration; $m = 2.34$, $k = 123$, $d_0 = 1.23$, $v_0 = 0$, $\omega_1 = 3.5$, $\omega_2 = 20$, $N = 4$

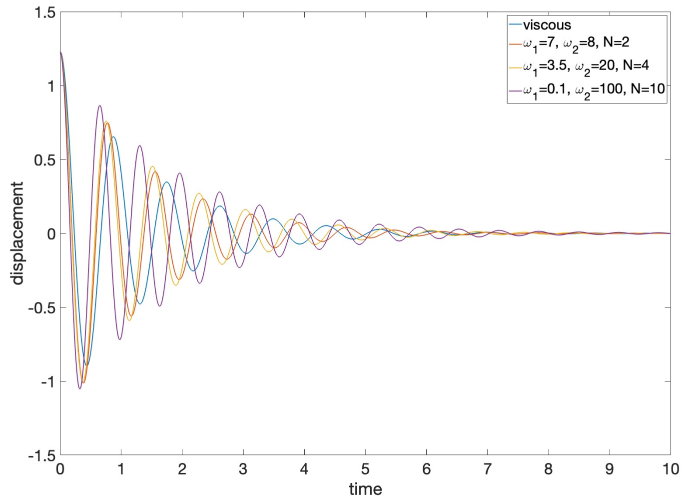

Fig. 5 Viscous Damping Ratio Comparison: effect of frequency bands.

Figure 6 compares the specific damping factor of this approach with the exact/viscous relation. Good agreement is seen with viscous damping in the frequency range of interest.

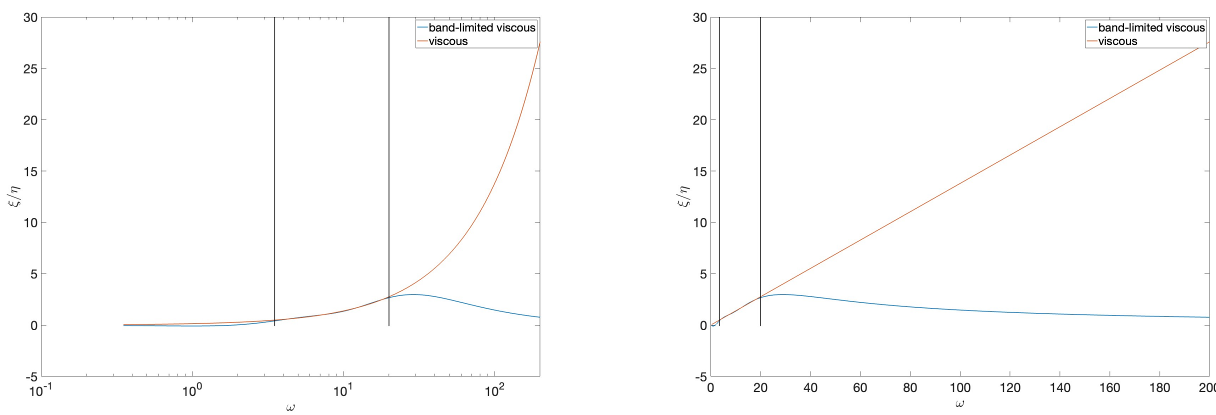

(a) Log scale.

(b) Linear scale.

Fig. 6 Specific damping factor scale: band-limited viscous damping[3].

Finally, fig. 7 compares viscous damping, the original band-limited damping approach, and the modified band-limited viscous approach as outlined above. The band-limited viscous results are a closer match for viscous damping, as expected.

Implementation

One important consideration when adopting this approach is the solution of eqs. (4) and (5). Here, we compare the ubiquitous forward and backward Euler approaches.

(Forward) Euler

We first divide the time domain into finite steps of length Δt. Subsequently, the solution to $\dot{y}(t) = g(t, y(t))$ at the ith

[3] $\omega_1 = 3.5$, $\omega_2 = 20$, $N = 4$

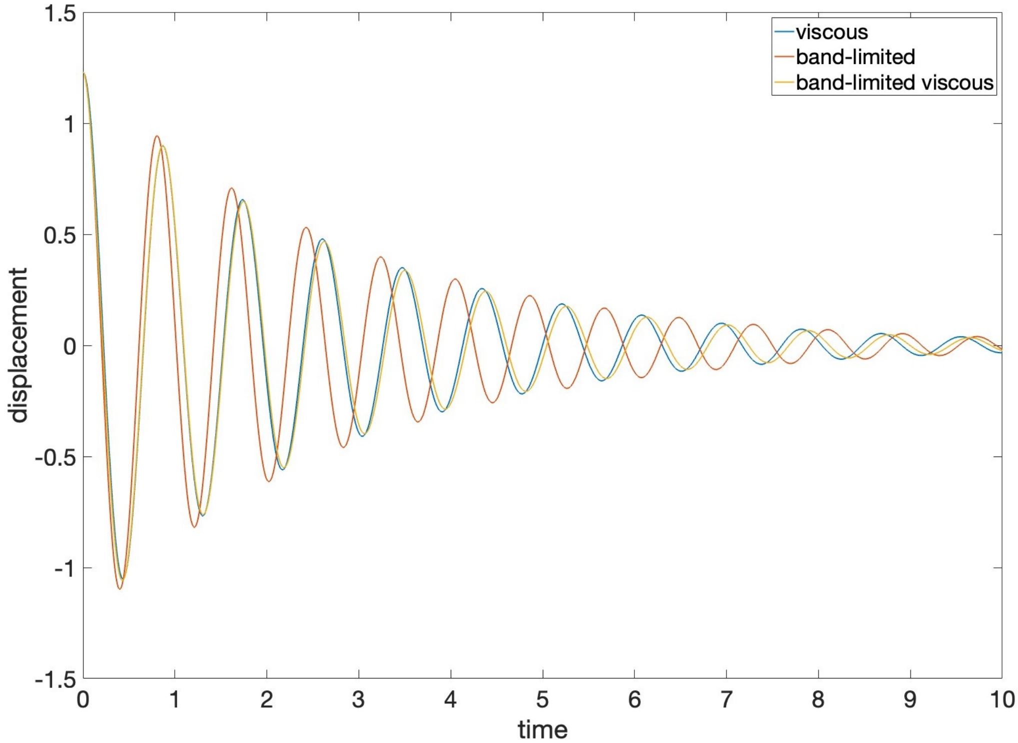

Fig. 7 Band-limited viscous comparison.

step may be approximated as:

$$y_i = y_{i-1} + \Delta t g(t_{i-1}, y_{i-1}) \tag{21}$$

Rearranging eq. (5), we obtain:

$$\dot{f}_{Ln}(t) = \omega_{cn} \left(f_0(t) - f_{Ln}(t) \right) \tag{22}$$

Applying Euler, we obtain:

$$\begin{aligned} f_{Ln(i)} &= f_{Ln(i-1)} + \Delta t \omega_{cn} \left(f_{0(i-1)} - f_{Ln(i-1)} \right) \\ &= f_{Ln(i-1)} + \Delta t \omega_{cn} \left(K d_{i-1} - f_{Ln(i-1)} \right) \end{aligned} \tag{23}$$

where we take $f_{Ln(0)} = 0$.

Finally, plugging the solution back into eq. (5) and then eq. (4), we can approximate the damping force as:

$$\begin{aligned} f_{d(i)} &= \eta \sum_1^N 2\alpha_n \frac{\dot{f}_{Ln(i)}}{\omega_{cn}} \\ &= \eta \sum_1^N 2\alpha_n \left[f_{0(i)} - f_{Ln(i)} \right] \\ &= \eta \sum_1^N 2\alpha_n \left[K d_i - f_{Ln(i-1)} - \Delta t \omega_{cn} \left(K d_{i-1} - f_{Ln(i-1)} \right) \right] \\ &= \eta \sum_1^N 2\alpha_n \left[K d_i - \Delta t \omega_{cn} K d_{i-1} - \left(1 - \Delta t \omega_{cn} \right) f_{Ln(i-1)} \right] \end{aligned} \tag{24}$$

Which leads to the following modified equations of motion at each step i:

$$M a_i + \hat{K} d_i = \hat{f}_{ext(i)} \tag{25}$$

where the modified stiffness $\hat{K}$ is defined as

$$\hat{K} = \left(1 + \eta \sum_{1}^{N} 2\alpha_n\right) K \tag{26}$$

and the external force is modified as:

$$\hat{f}_{ext(i)} = f_{ext(i)} + \eta \sum_{1}^{N} 2\alpha_n \left[\Delta t\omega_{cn} K d_{i-1} + (1 - \Delta t\omega_{cn})\, f_{Ln(i-1)}\right] \tag{27}$$

Backward Euler

While in forward Euler the values at the previous step are used to update the new solution, the backward Euler method uses values from the new solution to calculate the slope:

$$y_i = y_{i-1} + \Delta t g(t_i, y_i) \tag{28}$$

Again rearranging eq. (5) and applying backward Euler, we obtain:

$$f_{Ln(i)} = f_{Ln(i-1)} + \Delta t\omega_{cn} \left(K d_i - f_{Ln(i)}\right) \tag{29}$$

or

$$f_{Ln(i)} = \frac{f_{Ln(i-1)} + \Delta t\omega_{cn} K d_i}{1 + \Delta t\omega_{cn}} \tag{30}$$

where $f_{Ln(0)} = 0$.

As before, we can plug the solution back into eq. (5) and then eq. (4), and approximate the damping force as:

$$\begin{aligned} f_{d(i)} &= \eta \sum_{1}^{N} 2\alpha_n \frac{\dot{f}_{Ln(i)}}{\omega_{cn}} \\ &= \eta \sum_{1}^{N} 2\alpha_n \left[f_{0(i)} - f_{Ln(i)}\right] \\ &= \eta \sum_{1}^{N} 2\alpha_n \left[K d_i - \frac{f_{Ln(i-1)} + \Delta t\omega_{cn} K d_i}{1 + \Delta t\omega_{cn}}\right] \\ &= \eta \sum_{1}^{N} 2\alpha_n \frac{K d_i - f_{Ln(i-1)}}{1 + \Delta t\omega_{cn}} \end{aligned} \tag{31}$$

Leading to the following modified equations of motion:

$$M a_i + \hat{K} d_i = \hat{f}_{ext(i)} \tag{32}$$

where the modified stiffness $\hat{K}$ is defined as

$$\hat{K} = \left(1 + \eta \sum_{1}^{N} \frac{2\alpha_n}{1 + \Delta t\omega_{cn}}\right) K \tag{33}$$

and the external force is modified as:

$$\hat{f}_{ext(i)} = f_{ext(i)} + \eta \sum_{1}^{N} 2\alpha_n \frac{f_{Ln(i-1)}}{1 + \Delta t\omega_{cn}} \tag{34}$$

Note that with both approaches, this damping approach is represented in the governing equations as a stiffness modification and external force contribution. However, for linear systems, the forward Euler approach involves only an initial stiffness matrix modification (eq. (26)), and the damping force contribution and filtered force update (eqs. (23) and (27)) may be accomplished in a single call prior to the solution step. In contrast, the stiffness modification for the backward Euler approach (eq. (33)) involves the timestep Δt, which might change throughout the simulation, and the filtered force (eq. (30)) must be updated after the solution step, as it depends on the new displacement u_i.

While the backward Euler approach offers stability benefits at large time steps (fig. 8a), the forward Euler approach was ultimately chosen due to the implementation benefits outlined above. Below the critical timestep, the results for both approaches converge with decreasing timestep (figs. 8b to 8d).

[4]Spring-mass system in free vibration; $m = 2.34$, $k = 123$, $d_0 = 1.23$, $v_0 = 0$, $\zeta = 0.05$, $\omega_1 = 3.5$, $\omega_2 = 20$, $N = 4$, $\eta = 2\zeta = 0.1$

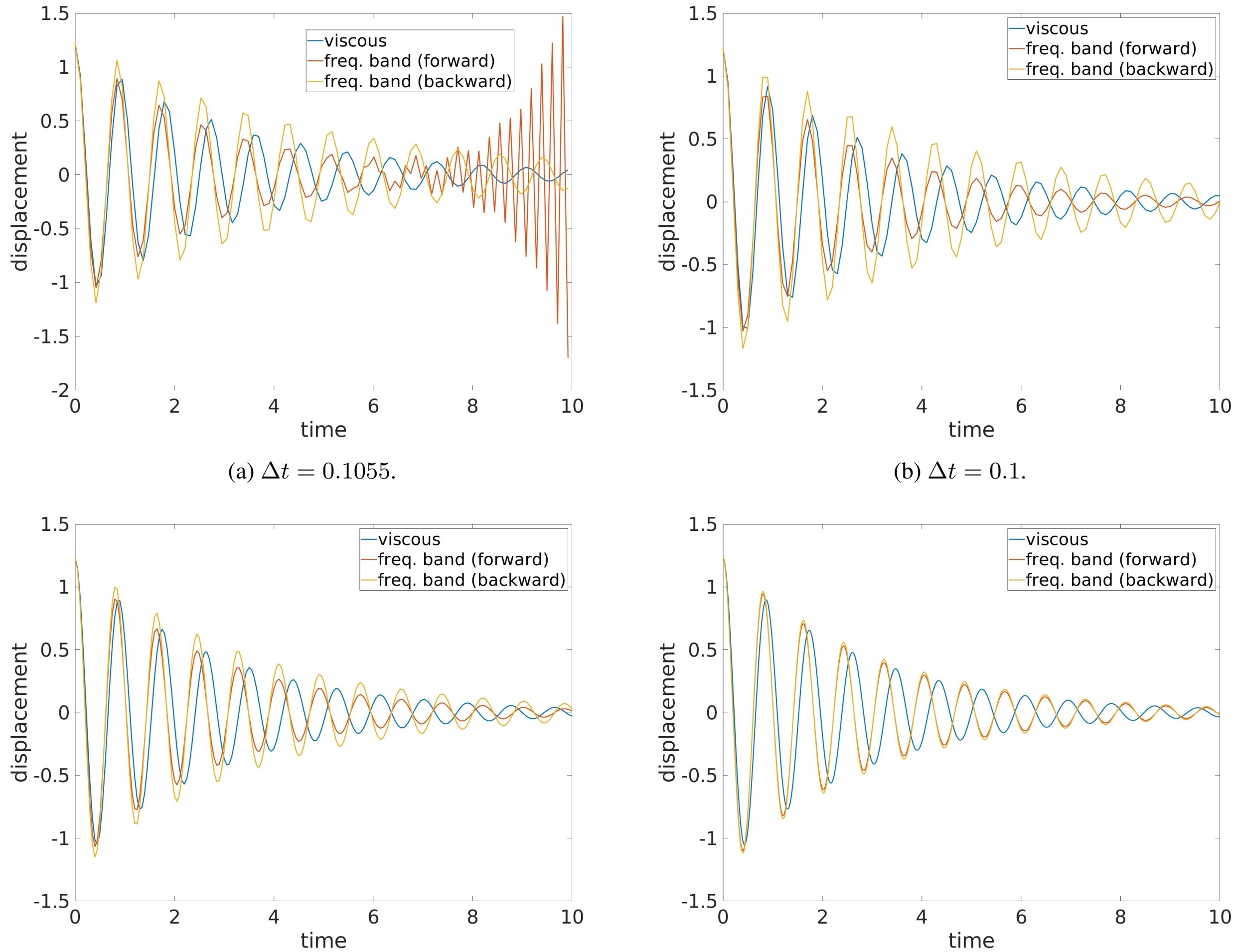

(a) $\Delta t = 0.1055$. (b) $\Delta t = 0.1$.

(c) $\Delta t = 0.05$. (d) $\Delta t = 0.01$.

Fig. 8 Comparison of forward and backward Euler for different time discretizations[4].

Results

We now examine some results for a large model, and offer some comparisons to modal damping approaches.

This model includes about 4 million elements, and was run on 800 parallel processors. While this example is fabricated, it has been tuned to be representative of the size and modal density of real models. Figure 9 shows several mode shapes of the model.

We will now use this model to compare the new band damping approach to direct modal damping. For modal damping, we further consider 2 approaches: direct transient simulation and modal transient (i.e., transient solution in the modal space). Note that even with a direct transient solution, an initial eigenvalue problem must still be conducted to compute modal information. For realistic system models with millions of degrees of freedom, the computation of modes can quickly become a performance bottleneck. Even worse, thousands of modes are often required to resolve the frequencies of interest, which frequently makes direct modal damping approaches prohibitively expensive. In this example, modal damping was limited to the first 5000 modes, which was enough to resolve frequencies up to around 7500 Hz (see fig. 10). In a direct transient simulation, this means that high-frequency content above 7500 Hz will be undamped. For modal transient simulations, high frequency content is zeroed.

In contrast, the new band-limited damping approach may be extended across an arbitrarily large frequency range with minimal overhead. In this example, we have damped frequencies up to 100,000 Hz, which would have been completely intractable using direct modal damping.

Figure 11 compares of the damping characteristics of each approach. Figure 11a plots the acceleration of a certain point

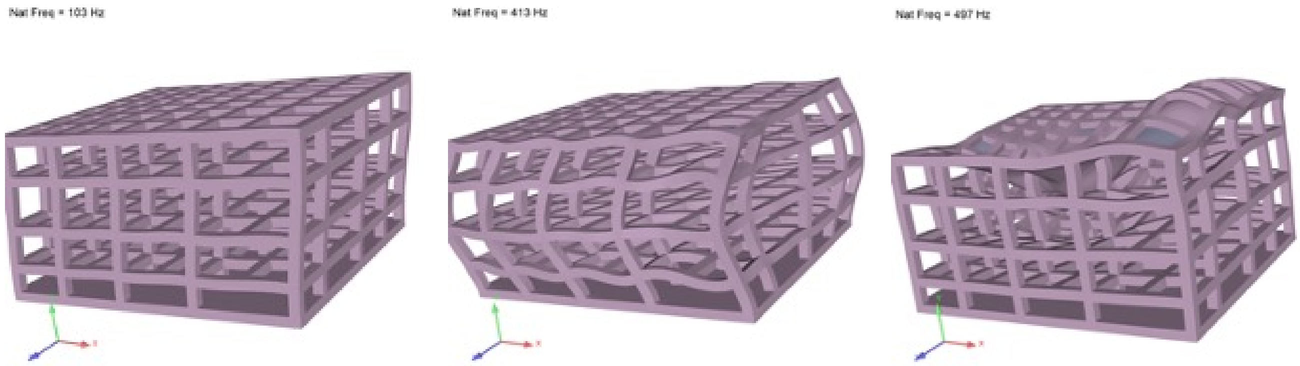

Fig. 9 Mode shapes of a large model.

over time, showing in broad strokes that all 3 approaches have similar damping characteristics. We also clearly see the lack of high-frequency content in the modal transient results. Figure 11b further reinforces this conclusion by examining frequency content. Below 7500 Hz, all 3 methods follow the same trends, with a slight shift between the modal and band damping approaches being attributable to the artificial stiffness contribution introduced by the band damping implementation (eq. (26)). Beyond the modal damping maximum of 7500 Hz they differ in the expected way, with modal damped transient trending more towards the undamped response, and modal transient results flattening out.

In table 1, we examine run times of a transient simulation, comparing both direct modal damping approaches with the new frequency band approach. The first 1 is a direct transient simulation with modal damping (10-7500 Hz). Column 2 is also a direct transient simulation, but with band-limited damping (10-100,000 Hz), and column 3 is a modal transient simulation with modal damping (10-7500 Hz). In all cases, the transient simulation included 20,000 steps, and a flat 2% damping was applied across the frequency range of interest.

Recall that the maximum frequency for modal damping is dictated by performance - uniform damping into the ultra-high-frequency range is completely untenable with this approach. However, even benefiting from a drastically reduced frequency

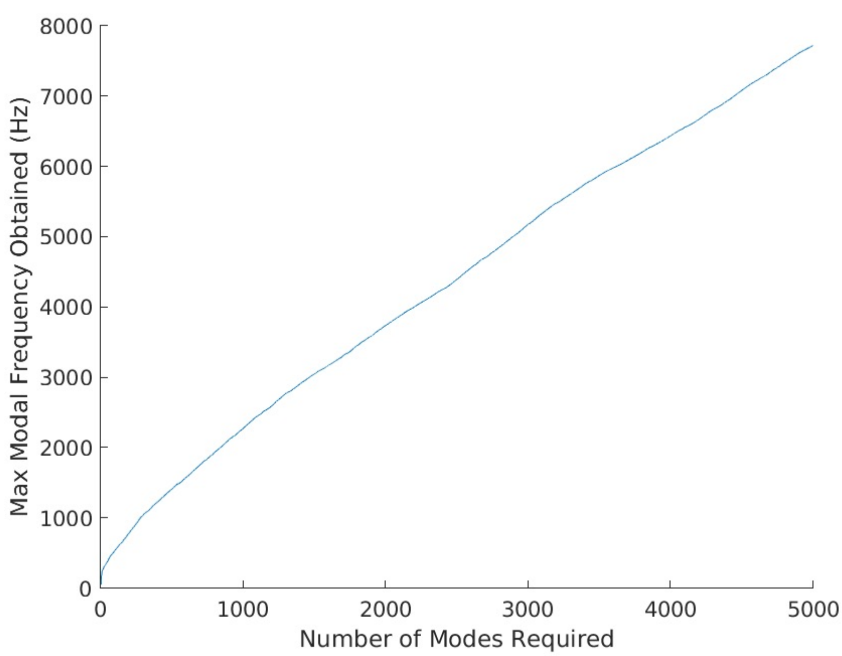

Fig. 10 Number of modes required to resolve a given frequency.

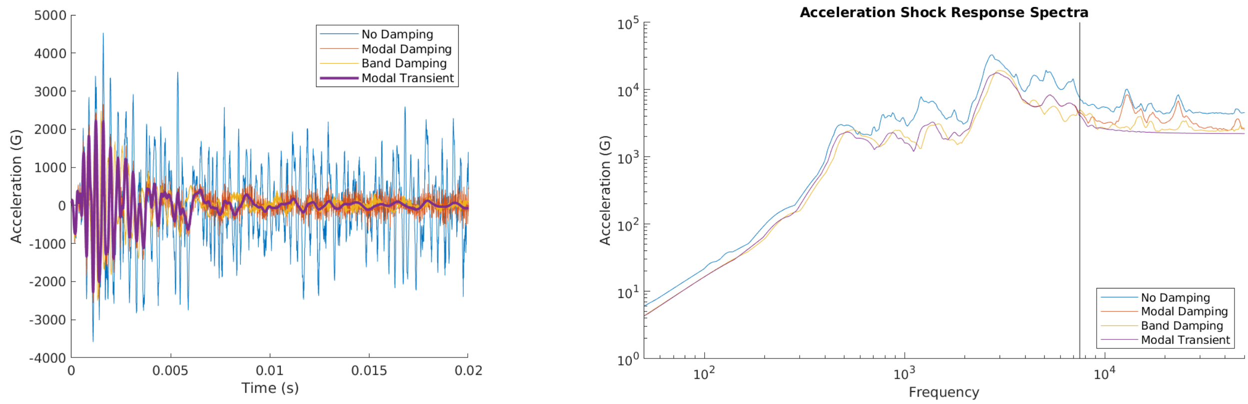

(a) Time domain.

(b) Frequency domain.

Fig. 11 Comparison of damping approaches.

Table 1 Runtime Comparison of Damping Approaches.

	Modal Damping (10 – 7500 Hz)	Band Damping (10 – 100000 Hz)	Modal Transient + Modal Damping
Compute Modes	46 hours	-	46 hours
Transient Simulation	12.0 hours	12.5 hours	0.2 hours
Total	58 hours	12.5 hours	46.2 hours

range, both modal damping approaches are still significantly slower than the new band damping approach. This is due to the huge upfront cost of calculating modes. Even after modal computation is complete, comparison of just the transient simulation times (row 2) shows that the addition of band damping only incurs a minor overhead over a direct transient simulation (12.5 vs. 12 hrs, or around 4%).

Conclusion

In conclusion, this damping approach offers a convenient and efficient way to apply uniform damping over a frequency range. For large simulations, this approach enjoys a significant advantage over direct modal damping, where thousands of modes might be required to capture engineering-relevant frequencies, leading to prohibitively expensive simulations. However, it suffers from slow decay of damping outside of the range of interest, which hampers its effectiveness, especially when multiple frequency bands are used in the same analysis. This effect can be mitigated somewhat by an alternative formulation proposed here, which introduces a tunable parameter to choose between a better fit within the range or faster decay outside.

Acknowledgments Sandia National Laboratories is a multi-mission laboratory managed and operated by National Technology & Engineering Solutions of Sandia, LLC (NTESS), a wholly owned subsidiary of Honeywell International Inc., for the U.S. Department of Energy's National Nuclear Security Administration (DOE/NNSA) under contract DE-NA0003525. This written work is authored by an employee of NTESS. The employee, not NTESS, owns the right, title and interest in and to the written work and is responsible for its contents. Any subjective views or opinions that might be expressed in the written work do not necessarily represent the views of the U.S. Government. The publisher acknowledges that the U.S. Government retains a non-exclusive, paid-up, irrevocable, world-wide license to publish or reproduce the published form of this written work or allow others to do so, for U.S. Government purposes. The DOE will provide public access to results of federally sponsored research in accordance with the DOE Public Access Plan.

Appendix A: Derivation of the Specific Damping Factor

Beginning from eqs. (4) and (5), one may derive the specific damping factor, eq. (6).

In the frequency domain, eqs. (4) and (5) become:

$$F_d(\omega) = \eta \sum_{1}^{N} i\omega \frac{2\alpha_n}{\omega_{cn}} F_{Ln}(\omega) \tag{35}$$

and

$$F_{Ln}(\omega) + i\omega \frac{F_{Ln}(\omega)}{\omega_{cn}} = F_0(\omega)$$

or (36)

$$F_{Ln}(\omega) = \frac{F_0(\omega)}{1 + i\left(\omega/\omega_{cn}\right)}$$

Substituting eq. (36) into eq. (35), we obtain

$$F_d(\omega) = \eta \sum_{1}^{N} 2\alpha_n i\left(\omega/\omega_{cn}\right) \frac{F_0(\omega)}{1 + i\left(\omega/\omega_{cn}\right)} \tag{37}$$

which can be manipulated via multiplication of both numerator and denominator by $(1 - i\left(\omega/\omega_{cn}\right))$ to

$$F_d(\omega) = \eta \sum_{1}^{N} 2\alpha_n \left[\frac{\left(\omega/\omega_{cn}\right)^2 - i\left(\omega/\omega_{cn}\right)}{1 + \left(\omega/\omega_{cn}\right)^2}\right] F_0(\omega) \tag{38}$$

Recalling that $f_{int}(t) = f_0(t) + f_d(t)$, we may state the resisting force in the frequency domain as

$$F_{int}(\omega) = \left[1 + \eta \sum_{1}^{N} 2\alpha_n \frac{\left(\omega/\omega_{cn}\right)^2}{1 + \left(\omega/\omega_{cn}\right)^2}\right] F_0(\omega) + i\eta \left[\sum_{1}^{N} 2\alpha_n \frac{\left(\omega/\omega_{cn}\right)}{1 + \left(\omega/\omega_{cn}\right)^2}\right] F_0(\omega) \tag{39}$$

And finally, following eqs. (2) and (3), the specific damping factor is found as

$$\xi(\omega) = \eta \sum_{1}^{N} 2\alpha_n \frac{\left(\omega/\omega_{cn}\right)}{1 + \left(\omega/\omega_{cn}\right)^2} \tag{40}$$

or equivalently as stated in eq. (6).

References

1. Huang, Yuli, Sturt, Richard, and Willford, Michael. "A damping model for nonlinear dynamic analysis providing uniform damping over a frequency range". Computers & Structures, 212 101–109 2019.
2. Beale, Dagny Marie, Bunting, Gregory, Day, David M., Dohrmann, Clark R., Lindsay, Payton, Pepe, Justin, and Plews, Julia Anne. "Sierra/SD – User's Manual – 5.18" URL: https://www.osti.gov/biblio/24300362024.
3. Chopra, Anil K. Dynamics of structures. Pearson Education India, 2007.